Chinese Chemical Letters 33 (2022) 907–911

Contents lists available at ScienceDirect

Chinese Chemical Letters

journal homepage: www.elsevier.com/locate/cclet

Oxygen-vacancy-rich phenanthroline/TiO_2 nanocomposites: An integrated adsorption, detection and photocatalytic material for complex pollutants remediation

Pinghua Chen[a,b], Huitao Zheng[a,b], Hualin Jiang[a,b,*], Jun Liu[a,b], Xinman Tu[a,b], Weibo Zhang[d], Bailey Phillips[c], Lei Fang[c,*], Jian-Ping Zou[a,b,*]

[a] Key Laboratory of Jiangxi Province for Persistent Pollutants Control and Resources Recycle, Nanchang Hangkong University, Nanchang 330063, China
[b] Department of Applied Chemistry, College of Environmental and Chemical Engineering, Nanchang Hangkong University, Nanchang 330063, China
[c] Department of Chemistry, Texas A&M University, College Station, Texas 77843, United States
[d] School of Resources, Environmental and Chemical Engineering, Nanchang University, Nanchang 330031, China

ARTICLE INFO

Article history:
Received 17 April 2021
Revised 25 May 2021
Accepted 1 July 2021
Available online 8 July 2021

Keywords:
Heavy metals
Organic contaminants
Adsorption
Detection
Photocatalytic degradation
Oxygen vacancy

ABSTRACT

To address the challenge of treating complex pollutants containing heavy metals and organic compounds, a phenanthroline/TiO_2 nanocomposite with rich oxygen vacancy defects was synthesized to integrate the functions of pollutant detection, adsorption, and photocatalytic degradation. The results showed that the nanocomposite could adsorb Cr^{3+} and the process could be transduced into a colorimetric signal for qualitative and quantitative detection. The adsorbed heavy metal also exhibited a synergistically enhanced photocatalytic degradation of a model organic pollutant under visible light. The simultaneous adsorption, detection, and photocatalysis could reduce the multifarious operations and high cost of traditional environmental remediation methods, indicating a strong application potential for the nanocomposite.

With the rapid development of human society, the increasing discharge of pollutants into the environment poses a serious hazard to all living things. Organic pollutants and heavy metals are among the most concerning contemporary contaminants due to their high toxicity and persistence in the environment. Consequently, methods for the detection and removal of these pollutants are important. Colorimetric detection has attracted much attention because it is intuitive and requires relatively simple instrumentation. Adsorption is widely used to remove heavy metals, and its low-cost and practicality make it suitable for use in rural and remote areas [1,2]. The photocatalytic removal of organic pollutants has seen rapid development in recent years due to its low cost, environmental-friendliness, and ease of operation [3-6].

Organic pollutants and heavy metals are two important classes of contaminants [7-9], and remediation strategies that only target one type of them are usually ineffective in treating complex pollution systems. Consequently, different methods are typically coupled together as a broad treatment strategy. However, the multiple treatment steps and materials employed result in tedious operations and high costs [10-12]. In this context, the emergence of novel multifunctional materials that couple high performance adsorption, detection and photocatalysis are exciting prospects for the future of environmental remediation technology. Oxygen vacancy defects can confer materials with beneficial properties, such as plentiful adsorption active sites, enhanced conductivity and suppression of electron-hole pair (e^--h^+) recombination. Accordingly, they have been widely engineered into adsorbents [13], detectors [14] and photocatalysts [15]. With this potential in mind, we envisaged that the introduction of oxygen vacancies could endow a material with the multifunctionality of adsorption, detection and photocatalysis.

With the aim to effectively treat organic and heavy metal contaminants, an oxygen-vacancy-rich nanocomposite of phenanthroline (Phen) modified TiO_2 (Phen/TiO_2) was synthesized by a facile single-step hydrothermal method. Methyl orange (MO) and Cr^{3+} were selected as the organic and heavy metal model contaminants due to their toxicity and ubiquity.

Scanning electron microscopy and transmission electron microscopy were used to analyze the nanoparticle morphology of Phen/TiO_2 (Figs. S2a and b in Supporting information). The ele-

* Corresponding authors.
E-mail addresses: hua20022000@126.com (H. Jiang), fang@chem.tamu.edu (L. Fang), zjp_112@126.com (J.-P. Zou).

https://doi.org/10.1016/j.cclet.2021.07.002
1001-8417/

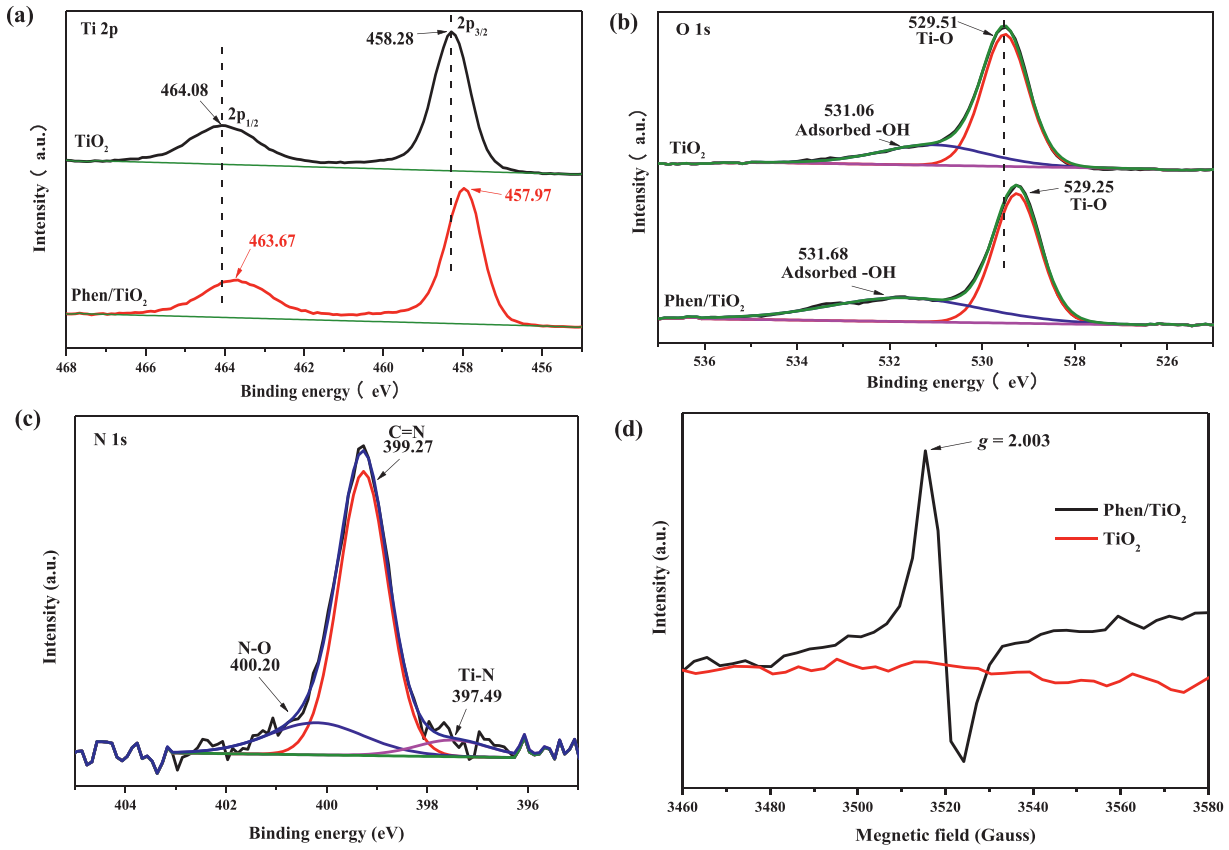

Fig. 1. High-resolution of XPS in the (a) Ti 2p, (b) O 1s regions of TiO_2 and Phen/TiO_2. (c) High-resolution of XPS in the N 1s region of Phen/TiO_2. (d) EPR spectra of Phen/TiO_2 and TiO_2.

mental mapping analysis (Figs. S2c-g in Supporting information) demonstrated that C, N, O and Ti were evenly distributed on the Phen/TiO_2 surface, suggesting the successful integration of Phen and TiO_2. The high-resolution X-ray photoelectron spectroscopy (XPS) spectra of the Ti 2p and O 1s regions of TiO_2 and Phen/TiO_2 exhibited a significant binding energy decrease in both Ti 2p and Ti–O of Phen/TiO_2 (Figs. 1a and b). This phenomenon indicated the existence of oxygen vacancies in Phen/TiO_2 [16]. The additional e^- remaining after the O atoms were removed from the surface of TiO_2 increases the e^- cloud density around the Ti and O atoms close to the oxygen vacancies, thus decreasing the binding energies of Ti and O [16]. The N 1s high-resolution XPS spectrum of Phen/TiO_2 could be resolved into three peaks at 397.49, 399.27 and 400.20 eV, corresponding to Ti–N, C=N and N–O, respectively (Fig. 1c) [17-18]. The N–O and C=N originated from adventitious organic compounds and phenanthroline, respectively. The N-Ti bond energies of Phen/TiO_2 indicate that the N atoms in phenanthroline were coordinated with the Ti atoms of TiO_2. This interaction between N and Ti may reduce the strength of the O–Ti bond in TiO_2, allowing the O atoms to leave, thereby promoting the formation of oxygen vacancies. To further confirm the existence of oxygen vacancies in Phen/TiO_2, an electron paramagnetic resonance (EPR) spectroscopy investigation was carried out. Fig. 1d shows the EPR spectra of Phen/TiO_2 and TiO_2. The EPR spectrum of Phen/TiO_2 exhibited a strong signal at $g = 2.003$, which was absent for TiO_2. This signal could be attributed to the e^- trapped in the oxygen vacancies and is strong evidence of their existence [19-20].

It was anticipated that Phen/TiO_2 would adsorb Cr^{3+} *via* chelation with the Lewis base N centers of Phen along with the electrostatic attraction from hydroxyl groups on the surface of TiO_2. The coordination event could be transduced into a colorimetric signal *via* metal-ligand charge transfer allowing the nanocomposite to operate as a chemosensor and an adsorbent. The isothermal and kinetic studies of Cr^{3+} adsorption by Phen/TiO_2 are given in Figs. S3 and S4 (Supporting information), and Tables S1 and S2 (Supporting infromation); the experimental details are given in Supporting information. The maximum adsorption capacity of Cr^{3+} was calculated to be 12.76 mg/g based on the Langmuir isotherm model, which is comparable with those of reported benchmark adsorbents for Cr^{3+} (Table S3 in Supporting Infromation). The kinetic study revealed *pseudo*-first order kinetic behavior (rate constant, $k = 1 \times 10^{-2}$ g mg^{-1} min^{-1}) depending on the concentrations of Cr^{3+} and Phen/TiO_2. In mixture of co-existing ions, Phen/TiO_2 exhibited high adsorption ability towards Cr^{3+}, indicating its highly selective adsorption performance (Fig. S8 in Supporting infromation).

To demonstrate the qualitative detection capability of Phen/TiO_2 towards Cr^{3+}, the nanocomposite was used to adsorb different metal ions, and its color-change was observed visually. Fig. 2a shows that the color of the Phen/TiO_2 nanocomposite was light yellow. When it captured Cr^{3+}, its color rapidly changed to green. The color-change was highly specific to Cr^{3+}. Other metal ions, such as Mn^{2+}, Zn^{2+}, Pb^{2+}, Co^{2+}, Ag^{+}, Cd^{2+}, Bi^{2+}, Ce^{2+}, Hg^{2+}, In^{2+}, Ni^{2+}, and Zr^{2+} did not induce a color change, while Fe^{3+} and $Cr_2O_7^{2-}$ induced color changes of red and bright yellow, respectively, even at concentrations five times than that of Cr^{3+}. These results demonstrated that Cr^{3+} could be visually and qualitatively detected by Phen/TiO_2. In order to quantitatively detect Cr^{3+}, Phen/TiO_2 was used to adsorb varying concentrations of Cr^{3+}. The chroma of Cr^{3+} adsorbed on Phen/TiO_2 was analyzed using visible-light difference diffuse reflectance spectroscopy (DRS). Fig. 2b shows the absorbance peak at $\lambda = 621$ nm from the dif-

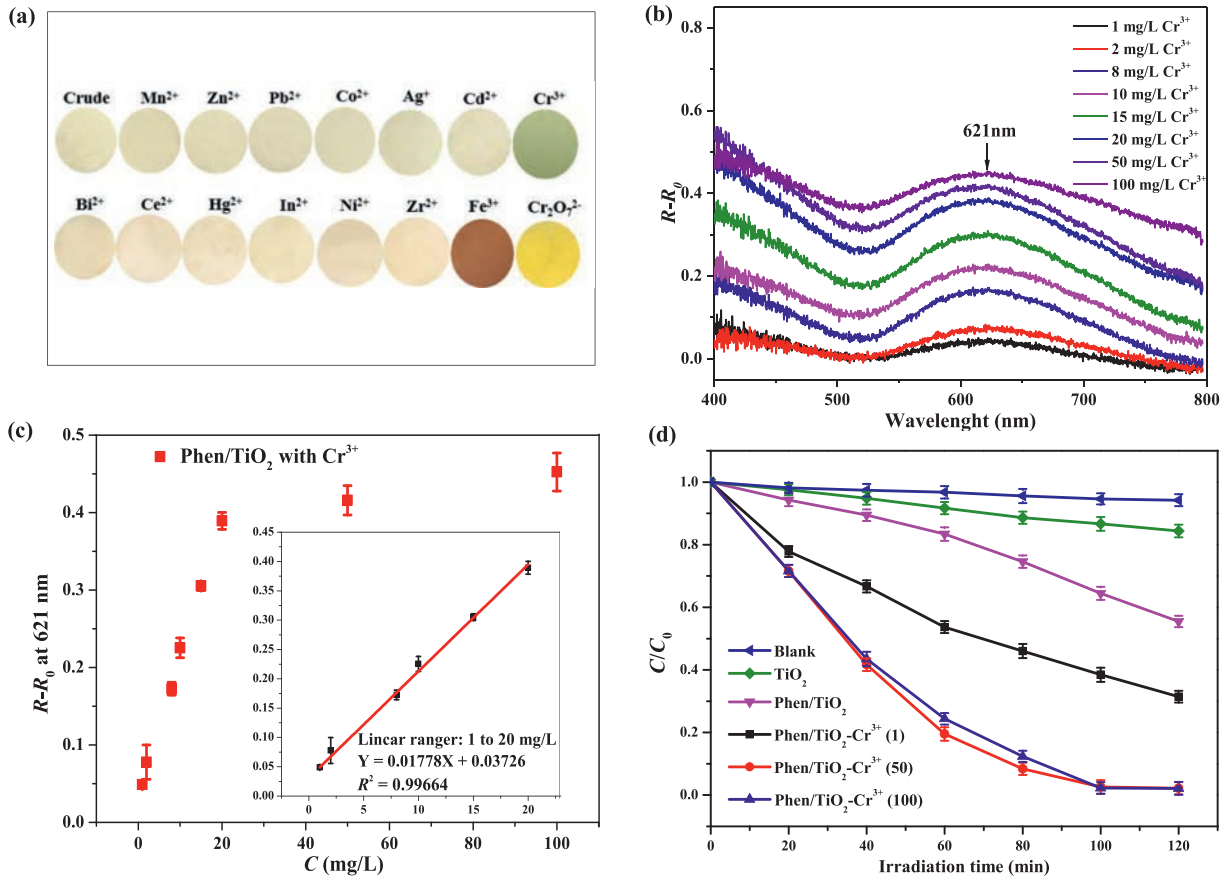

Fig. 2. (a) Photographic images of Phen/TiO_2 powders after being treated with different metal ions. Mn^{2+}, Zn^{2+}, Pb^{2+}, Co^{2+}, Ag^{+}, Bi^{2+}, Ce^{2+}, Hg^{2+}, In^{2+}, Ni^{2+}, Zr^{2+}, Fe^{3+}, $Cr_2O_7^{2-}$ and Cd^{2+}: 100 mg/L; Cr^{3+}: 20 mg/L; Adsorbent dosage: 1 g/L. (b) Concentration-dependent changes in visible difference DRS of Phen/TiO_2 during the detection of Cr^{3+}. (c) Concentration-dependent changes at λ = 621 nm (Adsorbent dosage was 1 g/L; The concentrations of Cr^{3+} were from 1 mg/L to 100 mg/L. Temperature was 30 °C, pH was 7. The experiments were performed in triple and the related error bars are indicated). (d) Photocatalytic degradation of MO over the bare TiO_2, Phen/TiO_2 and Phen/TiO_2-Cr^{3+} (The photocatalyst dosage was 1 g/L and the concentration of MO was 10 mg/L, room temperature.).

fuse reflectance spectra (DRS) of Cr^{3+} adsorbed Phen/TiO_2 at pH 7 and a temperature of 30 °C; the intensity of the peak at 621 nm increased with increasing concentration of Cr^{3+}. The intensity of the peak at 621 nm in the difference DRS was plotted against the Cr^{3+} concentration (Fig. 2c) and a linear relationship (calibration curve) was obtained over the concentration range 1-20 mg/L (insert in Fig 2c). Using this method, the Cr^{3+} concentration could be quantitatively determined from the color change of Phen/TiO_2 measured with DRS. The limit of detection (L_D) for Cr^{3+} was estimated to be 0.42 mg/L from the blank response according to Eq. 1:

$$L_D = \frac{KS_b}{m} \quad (1)$$

where $K = 3$, S_b was the standard deviation (SD) for the blank, and m was the slope of the linear calibration curve. The influence of pH, temperature and co-existing ions towards Phen/TiO_2 detecting Cr^{3+} are shown in Figs. S14-S16 (Supporting infromation).

To verify the accuracy of the colorimetric Cr^{3+} analysis obtained using the Phen/TiO_2 nanomaterial, the results were compared with those obtained by atomic absorption spectrometry (AAS) (Table S4 in Supporting Infromation). The relative standard deviation (SD) of the difference between the absolute values obtained by each method were < 3%, confirming the accuracy of the Phen/TiO_2-based method.

The bright color exhibited by the Cr^{3+} adsorbed Phen/TiO_2 (Phen/TiO_2-Cr^{3+}) indicated that the nanomaterial may possess enhanced light absorption capacity. It was envisioned that this feature could be exploited to enhance the photocatalytic activity, which could be applied to the degradation of organic pollutants. In this way, the adsorbed Cr^{3+} could act as a synergistic photocatalyst for the remediation of organic pollutants. To test this hypothesis, Phen/TiO_2 was pre-adsorbed with 1, 20, 50 and 100 mg/L of Cr^{3+} and used to photocatalytically degrade MO under visible light irradiation (Fig. 2d). Phen/TiO_2 exhibited higher photocatalytic capacity than TiO_2, indicating that the nanomaterial had enhanced visible light activity. Adsorption of Cr^{3+} onto Phen/TiO_2 further improved the photocatalytic activity. The photocatalytic degradation of MO increased as the Cr^{3+} concentration increased from 1 mg/L to 50 mg/L, reaching a plateau beyond 50 mg/L. Presumably the hyperchromic effect resulting from Cr^{3+} adsorption was almost saturated at a Cr^{3+} concentration of 50 mg/L, so further adsorption of Cr^{3+} had no additional influence. At an optimum Cr^{3+} adsorption of 50 mg/L, Phen/TiO_2-Cr^{3+} could degrade ~98% of 10 mg/L MO solution within 100 min.

The X-ray diffraction (XRD) patterns of the crystal phases of TiO_2, Phen/TiO_2, and Phen/TiO_2-Cr^{3+} are shown in Fig. S5 (Supporting infromation). The results showed that the incorporation of Phen changed the crystal phase of TiO_2 from pure anatase to mixed phases of anatase, rutile and brookite. Mixtures of different crystal phases of TiO_2 were shown to enhance visible light absorption due to the increased probability of forming heterojunctions in the TiO_2, thereby boosting the related photocatalytic performance [21]. To understand the mechanism of the increased photocatalytic activity demonstrated by the nanomaterial, the photo-

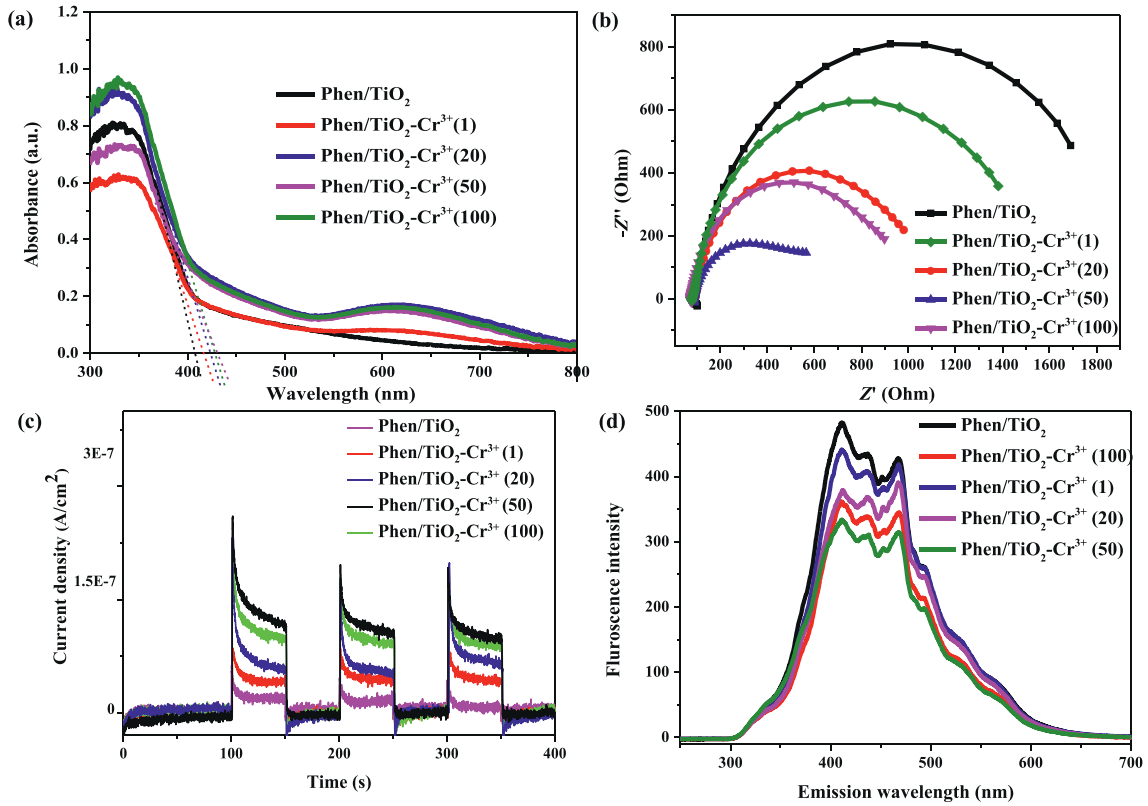

Fig. 3. (a) DRS of Phen/TiO_2 and Phen/TiO_2-Cr^{3+}. (b) Electrochemical impedance spectroscopy of Phen/TiO_2 and Phen/TiO_2-Cr^{3+}. (c) Photocurrent responses of Phen/TiO_2 and Phen/TiO_2-Cr^{3+} under visible light. (d) Photoluminescence spectra of Phen/TiO_2 and Phen/TiO_2-Cr^{3+}. The values in the brackets mean the feeding concentration (mg/L) of Cr^{3+} in the materials preparation.

electric properties of Phen/TiO_2 and Phen/TiO_2-Cr^{3+} were characterized. Fig. 3a shows that the dimensions of the light absorption edges of Phen/TiO_2, Phen/TiO_2-Cr^{3+} (1), Phen/TiO_2-Cr^{3+} (20), Phen/TiO_2-Cr^{3+} (50) and Phen/TiO_2-Cr^{3+} (100) were 408, 417, 423, 431 and 428 nm, respectively; (1), (20), (50) and (100) refer to the concentrations (mg/L) of adsorbed Cr^{3+}. The hyperchromicity resulting from the adsorption of Cr^{3+} produced a redshift of the absorption edge of Phen/TiO_2. However, when the concentration of Cr^{3+} was > 50 mg/L the hyperchromicity was saturated and the redshift of the adsorption edge ceased. These observations were consistent with the results of the photocatalytic degradation experiments. The nanomaterials were additionally characterized by electrochemical impedance spectroscopy (EIS) (Fig. 3b). Phen/TiO_2 exhibited the highest impedance. The impedance decreased with the addition of Cr^{3+} over the concentration range 1-50 mg/L but increased at concentrations > 50 mg/L Cr^{3+}. In other words, Phen/TiO_2 in the presence of 50 mg/mL Cr^{3+} exhibited the smallest impedance among the samples, suggesting that the adsorption of Cr^{3+} significantly decreased the impedance of Phen/TiO_2 [22]. The photocurrent (PC) spectroscopy responses and photoluminescence (PL) spectra of the samples are shown in Figs. 3c and d. Compared with EIS, the PC responses and PL spectra exhibited similar trends following Cr^{3+} adsorption by Phen/TiO_2. The corresponding photo-electronic properties of the samples increased with the increasing Cr^{3+} adsorption to reach maximum values at a Cr^{3+} concentration of 50 mg/L and decreased thereafter. The magnitude of the current density in PC spectra reflects the number of e^- produced in the sample by light irradiation [23]. In PL spectra, a low fluorescence intensity is indicative of the slow recombination rate of photo-generated charge carriers [24]. Phen/TiO_2-Cr^{3+}(50) had the highest PC density and lowest PL intensity.

To determine the active species in the degradation of MO, various scavengers were added to the photocatalysis system. The results given in Fig. S6 (Supporting infromation) indicated that h^+ and $^{\bullet}O_2^-$ are the important active species in the degradation of MO while e^- and $^{\bullet}OH$ play a minor role.

Based on these results, a mechanism for the photocatalytic degradation of MO by Phen/TiO_2-Cr^{3+} under visible light was proposed: Although pure anatase TiO_2 cannot be excited under visible light, the incorporation of Phen modified the crystal phase of TiO_2 from pure anatase to mixed phases of anatase, rutile and brookite; visible light absorbed by the modified phase could now excite e^- from the valence band (VB) to the conduction band (CB) leaving h^+ (on the VB) [21,25]. Furthermore, the hyperchromic effect resulting from the N-chelation of Cr^{3+} by Phen enhanced the absorption of visible light, while also decreasing the impedance, which facilitated the photo-generation of charge carriers and depressed the recombination of charge carriers, all boosting the photocatalytic performance [26]. The photo-generated e^- in the CB could then react with O_2 to produce $^{\bullet}O_2^-$, which oxidized and degraded MO. The photo-generated h^+ on the VB could also oxidize and degrade the pollutant.

An oxygen-vacancy-rich nanocomposite of Phen/TiO_2, integrating the functions of detection, adsorption, and photocatalytic degradation of pollutants, was successfully prepared by a facile one-step hydro-thermal method. Phen/TiO_2 could simultaneously adsorb and detect Cr^{3+} while the adsorbed heavy metal could synergistically enhance the photocatalytic degradation of MO under visible light irradiation. The integrated multi-functionality of the Phen/TiO_2 demonstrated that these nanomaterials may offer a credible and efficient alternative to traditional adsorbents used for the remediation of complex pollutants. The strategy developed here may also provide a new outlook for the design of functional materials for practical applications.

Declaration of competing interest

The authors declare that they have no known competing financial interests or personal relationships that could have appeared to influence the work reported in this paper.

Acknowledgments

The project is supported by the National Natural Science Foundation of China (Nos. 51978323, 42077162), the Key Research and Development Project of Jiangxi Province (No. 20203BBGL73229), and the Natural Science Foundation of Jiangxi Province (No. 20192ACBL20042).

Supplementary materials

Supplementary material associated with this article can be found, in the online version, at doi:10.1016/j.cclet.2021.07.002.

References

[1] Q. Wang, P. Chen, X. Zeng, J. Hazard. Mater. 381 (2020) 120954.
[2] D. Kang, X. Yu, M. Ge, Chem. Eng. J. 330 (2017) 36–43.
[3] X.F. Wu, Y. Sun, H. Li, J. Alloys Compd. 740 (2018) 1197–1203.
[4] H. Jiang, X. Li, M. Li, Chem. Eng. J. 358 (2019) 58–66.
[5] S. Zhang, J. Yi, J. Chen, Chem. Eng. J. 380 (2020) 122583.
[6] C. Cheng, S. Zong, J. Shi, Appl. Catal. B: Environ. 265 (2020) 118620.
[7] C. Liu, Y. Ding, W. Wu, Y. Teng, Chem. Eng. J. 306 (2016) 22–30.
[8] F. Li, J. Huang, Q. Xia, Sep. Purif. Technol. 195 (2018) 83–91.
[9] W. Ding, J. Shi, W. Wei, C. Cao, H. Jiu, Int. J. Hydrog. Energy 46 (2021) 2899–2904.
[10] P.A. Neale, C. Feliers, L. Glauch, Environ. Sci. Wat. Res. 9 (2020) 2444–2453.
[11] J.J. Alvear-Daza, J. Sanabria, H.M. Gutiérrez-Zapata, J.A. Rengifo-Herrera, Sol. Energy 176 (2018) 581–588.
[12] M. Li, S. Zhou, Y. Xu, Chem. Eng. J. 334 (2018) 1621–1629.
[13] 13.F. Ma, J. Yao, Y. Zhang, Y Wei, Chin. Chem. Lett. 29 (2018) 1689–1691.
[14] Z. Ni, S. Bao, X. Gong, Chin. Chem. Lett. 31 (2020) 1674–1679.
[15] X. Xie, Q.U. Hassan, H. Lu, Chin. Chem. Lett. 32 (2021) 2038–2042.
[16] Z. Hu, K. Lia, X. Wu, Appl. Catal. B: Environ. 256 (2019) 117860.
[17] K. Batalović, N. Bundaleski, J. Radaković, Phys. Chem. Chem. Phys. 19 (2017) 7062.
[18] Y. Wang, C. Feng, M. Zhang, J. Yang, Z. Zhang, Appl. Catal. B: Environ. 100 (2010) 84–90.
[19] Z. Sun, R. Huo, C. Choi, Nano Energy 62 (2019) 869–875.
[20] B. Wang, M. Zhang, X. Cui, Angew. Chem. Int. Ed. 132 (2020) 1628–1635.
[21] Y. Chu, L. Gu, H. Du, Int. J. Hydrog. Energ. 43 (2018) 21810–21823.
[22] J. Chen, J. Zhan, Y. Zhang, Y. Tang, Chin. Chem. Lett. 30 (2019) 735–738.
[23] H. Jiang, J. Liu, M. Li, Chinese J. Catal. 39 (2018) 747–759.
[24] H. Jiang, M. Li, J. Liu, Ceram. Int. 44 (2018) 2709–2717.
[25] K. Chalastara, F. Guo, S. Elouatik, Catalysts 10 (2020) 407.
[26] Y. Shen, C. Zhu, B. Chen, Environ. Sci. Nano 7 (2020) 1525–1538.